Mathematical Modelling and Control

https://www.aimspress.com/journal/mmc

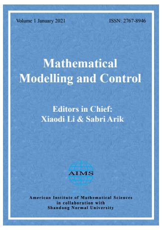

MMC, 6(2): 151–162.
DOI: 10.3934/mmc.2026012
Received: 17 December 2024
Revised: 05 March 2025
Accepted: 22 March 2025
Published: 28 May 2026

Research article

Predefined-time formation control for QUAV under input saturation

Mengcheng Wang[1], **Shu Zhang**[2,*] **and Dengxiu Yu**[3]

[1] Sanya Oceanographic Institution, Ocean University of China, Sanya, Hainan 572000, China; wangmengcheng@mail.nwpu.edu.cn

[2] Information Science and Engineering, Ocean University of China, Qingdao, Shandong 266100, China

[3] School of Artificial Intelligence, OPtics and ElectroNics (iOPEN), Northwestern Polytechnical University, Xian, Shanxi 710072, China

* **Correspondence:** Email: zhangshu@ouc.edu.cn.

Abstract: This paper investigates the predefined-time formation control of quadrotor unmanned aerial vehicles (QUAVs) under input saturation constraints. To mitigate the effects of input saturation, an auxiliary system is meticulously designed. In contrast to other studies which merely attain the asymptotic stability of the auxiliary signals, the auxiliary system proposed ensures the predefined-time stability, thus contributing the stability of entire system. Subsequently, based on the predefined-time stability criterion, a distributed formation controller is developed, thus guaranteeing the predefined-time stability and robustness of formation under input saturation. Finally, simulations validate the effectiveness of the proposed method.

Keywords: QUAV formation; predefined-time control; input saturation; auxiliary system

1. Introduction

In recent years, multi-agent systems (MAS) have emerged as an effective solution for complex tasks due to their efficiency, low cost, flexibility, and reliability [1]. Quadrotor unmanned aerial vehicle (QUAV) formation control, as a promising application of MAS, has been widely adopted in search and rescue operations [2], traffic monitoring [3], and agricultural spraying [4]. As QUAV formation (QUAVF) systems adapt to complex environments and tasks, higher flight performance standards are required. Physical properties and safety factors must also be considered. In particular, input variables such as thrust and torque must be limited to ensure vehicle safety and proper operation [5]. Despite some studies having achieved rapid convergence in formations under input saturation, they often lack the ability to arbitrarily set the convergence times. Moreover, while much existing research on formation control has been conducted, it has overlooked input saturation, thus risking performance degradation and safety. Therefore, our study aims to fill this significant research gap by investigating the predefined-time formation control of QUAVs under input saturation constraints.

Considering QUAVF adaptation to complex environments and tasks, the ability for rapid convergence in QUAVF control becomes crucial to ensure both safety and successful execution. To enhance the convergence speed, finite-time formation control has been explored [6]. Several studies [7–11] have focused on achieving the desired formations in finite time, but the stability time depends on the initial conditions and design parameters [12]. In contrast to finite-time stability, fixed-time stability [13] offers faster convergence rates, and the upper limit of stability time can be estimated. The exploration and application of fixed-time control for QUAVF have been investigated [14–17]. Despite the advantages of fixed-time control in estimating the stability time, determining the explicit relationship between the settling time and the system parameters remains challenging. The predefined-time control (PTC) method allows QUAVs to quickly form formations and maintain stable flights within a user-defined timeframe [18]. Unlike other approaches where the convergence time depends on various design parameters and the initial conditions, PTC simplifies this by depending on one control parameter, which is the predefined time. This dependency not only streamlines the tuning process but also enhances the predictability and control over the system's behavior, thus facilitating easier adjustments to meet specific operational needs. In [19], an innovative practical predefined-time stability criterion was proposed, which provides clearer guidance for the design of the PTC. Studies on predefined-time consensus tracking [20] and adaptive PTC for QUAVF [21] have been presented, but none simultaneously considered input saturation effects.

In actual QUAVF control, input variables such as thrust and torque are finite due to physical limitations, such as exceeding limits leading to motor overheating, battery drain, and structural damage, thus degrading the performance and posing hazards. Neglecting the constraints posed by input saturation can result in control inputs that far exceed the available actuation capabilities, leading to significant degradation of the control performance and potentially catastrophic failures. Research on adaptive neural networks [22, 23] and auxiliary systems [24] has addressed actuator constraints. Continuous theoretical advancements [25, 26] have been made for single QUAVs. For collective control, Wang et al. [27] investigated tracking problems under input constraints, while [28] designed an input saturation auxiliary system to mitigate the effects of input saturation. [29] studied the flight formation control problem of QUAVF with bounded control thrust, yet rapid convergence time control schemes were not designed. Although input saturation has been addressed in finite-time and fixed-time control studies [30,31], these methods do not allow users to set stabilization time bounds.

To the best of our knowledge, there exists a significant research gap in the existing literature regarding the integration of PTC with input saturation considerations of QUAVF. Our research targets these issues, and the main contributions of our work are as follows:

1) This research endeavors to fulfill the requirement of maintaining predefined-time stability in QUAVF even under input saturation constraints. Although the PTC of QUAVF has been investigated in previous studies [20, 21], the input saturation has been overlooked. To bridge this gap, this work presents an integrated framework that incorporates both aspects, thus enhancing the overall reliability and practicality of the system.

2) A QUAVF control method is proposed that guarantees system stability within a predefined time under input saturation. Unlike previous approaches [30, 31] that concentrated on finite-time and fixed-time control with convergence time depending on the initial states and complex parameters, this method provided the flexibility for users to prescribe the upper bound of the stabilization time, thus achieving predefined-time stability.

3) To mitigate the adverse effects of input saturation, an innovative predefined-time auxiliary system is designed and incorporated into the QUAVF controller. While auxiliary systems in [30–32] can only achieve asymptotic stability of the auxiliary signals, the proposed auxiliary system achieves predefined-time stability, ultimately contributing to the stability of the entire closed-loop system.

The structure of this paper is as follows: in Section 2, we present the fundamental concepts of predefined-time stability and establish the mathematical groundwork; subsequently, Section 3 focuses on the design of the controller tailored for input-saturated scenarios and conducts a comprehensive stability analysis; to validate the efficacy of our proposed control design, Section 4 demonstrates its correctness and practicality; finally, in Section 5, we not only summarize the key findings and contributions of this research but also offer insights into the potential future research directions, thus paving the way for further investigations in this field.

2. Preliminaries and problem formulation

2.1. System dynamic

Consider the following QUAVF system, where the leader is designated as 1 and the followers are numbered from 2 to N. According to [33], the dynamics of a QUAV can be described by the following:

$$
\begin{cases}
\ddot{x}_i = \frac{\mathcal{T}_i}{m_i}\left(S(\theta_i)C(\psi_i)C(\phi_i) + S(\psi_i)S(\phi_i)\right) - \frac{\mathcal{K}_{i,x}}{m_i}\dot{x}_i + \mathcal{D}_{i,x},\\
\ddot{y}_i = \frac{\mathcal{T}_i}{m_i}\left(S(\theta_i)S(\psi_i)C(\phi_i) - C(\psi_i)S(\phi_i)\right) - \frac{\mathcal{K}_{i,y}}{m_i}\dot{y}_i + \mathcal{D}_{i,y},\\
\ddot{z}_i = \frac{\mathcal{T}_i}{m_i}C(\theta_i)C(\phi_i) - \mathrm{g} - \frac{\mathcal{K}_{i,z}}{m_i}\dot{z}_i + \mathcal{D}_{i,z},\\
\ddot{\phi}_i = \frac{\mathcal{J}_{i,\phi}}{\mathcal{I}_{i,x}} + \frac{\mathcal{I}_{i,y}-\mathcal{I}_{i,z}}{\mathcal{I}_{i,x}}\dot{\theta}_i\dot{\psi}_i - \frac{\mathcal{I}_{i,R}\mathcal{K}_{i,\phi}}{\mathcal{I}_{i,x}}\dot{\phi}_i + \mathcal{D}_{i,\phi},\\
\ddot{\theta}_i = \frac{\mathcal{J}_{i,\theta}}{\mathcal{I}_{i,y}} + \frac{\mathcal{I}_{i,z}-\mathcal{I}_{i,x}}{\mathcal{I}_{i,y}}\dot{\phi}_i\dot{\psi}_i - \frac{\mathcal{I}_{i,R}\mathcal{K}_{i,\theta}}{\mathcal{I}_{i,y}}\dot{\theta}_i + \mathcal{D}_{i,\theta},\\
\ddot{\psi}_i = \frac{\mathcal{J}_{i,\psi}}{\mathcal{I}_{i,z}} + \frac{\mathcal{I}_{i,x}-\mathcal{I}_{i,y}}{\mathcal{I}_{i,z}}\dot{\phi}_i\dot{\theta}_i - \frac{\mathcal{I}_{i,R}\mathcal{K}_{i,\psi}}{\mathcal{I}_{i,z}}\dot{\psi}_i + \mathcal{D}_{i,\psi},
\end{cases}
\tag{2.1}
$$

where x_i, y_i, z_i represent the positions, and ϕ_i, θ_i, ψ_i denote the attitude angles. $\mathcal{I}_{i,R}$ is the distance from the center of mass to the center of the rotor, and $\mathcal{I}_{i,x}-\mathcal{I}_{i,z}$ are the moments of inertia. The coefficients $\mathcal{K}_{i,x}-\mathcal{K}_{i,\psi}$ represent aerodynamic damping. m_i is the mass, and g is gravitational acceleration. The disturbances are $\mathcal{D}_{i,x} - \mathcal{D}_{i,\psi}$. The thrust $\mathcal{T}_i$ and control torques $\mathcal{J}_{i,\phi}, \mathcal{J}_{i,\theta}, \mathcal{J}_{i,\psi}$ are also included. The virtual leader's dynamics are described by time-varying signals $x_d(t)-\psi_d(t)$. Additionally, S represents sine (i.e., $S(\theta) = \sin(\theta)$), and C represents cosine (i.e., $C(\theta) = \cos(\theta)$).

2.2. Communication topology

A leader - follower formation control [34,35] architecture is adopted, where UAV1 serves as the leader and the remaining UAVs are followers. The system's interaction topology is comprised of two components: communication among followers and information flow from the leader to followers.

Let $\mathscr{G} = \{\mathscr{V}, \mathscr{E}, \mathscr{A}\}$ be the communication graph of followers. Here, $\mathscr{V} = \{v_1, v_2, \ldots, v_m\}$ represents the node set, $\mathscr{E} \subseteq \mathscr{V} \times \mathscr{V}$ is the edge set, and $\mathscr{A} = [a_{ij}]_{m\times m} \in \mathbb{R}^{m\times m}$ is the weighted adjacency matrix with $a_{ij} \geq 0$ for $i, j = 1, 2, \ldots, m$. An edge $(v_i, v_j) \in \mathscr{E}$ implies that node v_i can receive information from v_j, and $a_{ij} \neq 0$ if and only if $(v_i, v_j) \in \mathscr{E}$. An undirected communication topology is assumed (i.e., $(v_i, v_j) \in \mathscr{E}$ if and only if $(v_j, v_i) \in \mathscr{E}$).

Based on the weighted adjacency matrix $\mathscr{A}$, the Laplacian matrix $L = [l_{ij}]_{m\times m} \in \mathbb{R}^{m\times m}$ is defined as follows:

$$
l_{ij} = \begin{cases} \sum_{k=1}^{m} a_{ik}, & i = j, \\ -a_{ij}, & i \neq j. \end{cases} \tag{2.2}
$$

The leader - follower interaction is represented by a diagonal matrix $B = \mathrm{diag}\{b_1, \ldots, b_m\}$, where $b_i > 0$ means follower i can directly receive leader information, and $b_i = 0$ otherwise. This topology enables internal cohesion among followers and synchronized tracking of the leader's trajectory, thus allowing the QUAVF to perform cooperative tasks effectively.

2.3. Radial basis function neural network (RBF-NN)

There are many nonlinear functions that are difficult to represent in the six-degree-of-freedom dynamics model of the QUAV, and many complex nonlinear functions are introduced during the control design process [36, 37]. In order to facilitate the design of the predefined-time control algorithm, a function approximator is introduced to approximate the nonlinear functions. Currently commonly used function approximators are radial basis function neural network (RBF-NN) and fuzzy logic systems, this paper uses RBF-NN to fit the nonlinear function, which is briefly described as follows.

RBF-NN is a function approximator and widely used in controller design. In this article, it is utilized to fit an unknown and continuous nonlinear function $F(X)$, with the following formula holding:

$$
F(X) = W^T S(X) + \varepsilon(X), \tag{2.3}
$$

where $W \in \mathbb{R}^{(l\times q)}$ represents the ideal weight of the neural network, $S(X) \in \mathbb{R}^l$ is the output vector, and l denotes the number of neurons. The approximation error, $\varepsilon(X) \in \mathbb{R}^q$, satisfies $\|\varepsilon(X)\| \leq \varepsilon^*$, where ε^* denotes an unknown positive constant.

The basic function of RBF-NN is defined as follows:

$$
s_i(X) = exp\left(\frac{-\|X - c_i\|^2}{2\sigma_i^2}\right), \tag{2.4}
$$

where $\sigma_i > 0$ denotes the width parameter of the i-th neuron, $c_i = [c_{i1}, \ldots, c_{ip}]^T$ denotes the central value.

2.4. Problem formulation

Given the physical constraints on the actuators of QUAVs, the issue of input constraints cannot be ignored. To address these input constraints, we first transform the QUAV dynamics model (2.1) into a more simplified form:

$$
\begin{cases} \dot{p}_{i,\tau} = v_{i,\tau}, \\ \dot{v}_{i,\tau} = g_\tau u_{i,\tau} + f_{i,\tau} + d_{i,\tau}, \end{cases} \tag{2.5}
$$

where τ represents any of the variables $x_i, y_i, z_i, \psi_i, \phi_i, \theta_i$ for $i = 1, 2, \dots, N$. The position components, denoted as $p_{i,\tau}$, correspond to x_i, y_i, z_i, ϕ_i, θ_i, ψ_i respectively; the velocity components, represented as $v_{i,\tau}$, correspond to $\dot{x}_i$, $\dot{y}_i$, $\dot{z}_i$, $\dot{\phi}_i$, $\dot{\theta}_i$, $\dot{\psi}_i$ respectively. The gravitational coefficients are given as $g_{i,\tau} = \frac{1}{m_i}$ for position axes and $\frac{1}{\mathcal{I}_{i,\tau}}$ for attitude axes.

The damping forces consist of two parts. For translational motion, they are expressed as $f_{i,x} = -\frac{\mathcal{K}_{i,x}}{m_i}\dot{x}_i$, $f_{i,y} = -\frac{\mathcal{K}_{i,y}}{m_i}\dot{y}_i$, and $f_{i,z} = -\frac{\mathcal{K}_{i,z}}{m_i}\dot{z}_i - mg$. For rotational motion, the attitude damping terms are described by $f_{i,\phi} = \frac{\mathcal{I}_{i,y}-\mathcal{I}_{i,z}}{\mathcal{I}_{i,x}}\dot{\theta}_i\dot{\psi}_i - \frac{\mathcal{I}_{i,R}\mathcal{K}_{i,\phi}}{\mathcal{I}_{i,x}}\dot{\phi}_i$, $f_{i,\theta} = -\frac{\mathcal{I}_{i,z}-\mathcal{I}_{i,x}}{\mathcal{I}_{i,y}}\dot{\phi}_i\dot{\psi}_i - \frac{\mathcal{I}_{i,R}\mathcal{K}_{i,\theta}}{\mathcal{I}_{i,y}}\dot{\theta}_i$, and $f_{i,\psi} = \frac{\mathcal{I}_{i,x}-\mathcal{I}_{i,y}}{\mathcal{I}_{i,z}}\dot{\phi}_i\dot{\theta}_i - \frac{\mathcal{I}_{i,R}\mathcal{K}_{i,\psi}}{\mathcal{I}_{i,z}}\dot{\psi}_i$. $\mathcal{D}_{i,\tau}$ represents the external disturbances.

After obtaining the control input $\upsilon_{i,\tau}$, the relationship between control inputs, total thrust, and torques is given by the following:

$$\begin{cases} u_{i,x} = (S(\theta_i)C(\psi_i)C(\phi_i) + S(\psi_i)S(\phi_i))\mathcal{T}_i, \\ u_{i,y} = (S(\theta_i)S(\psi_i)C(\phi_i) - C(\psi_i)S(\phi_i))\mathcal{T}_i, \\ u_{i,z} = C(\theta_i)C(\phi_i)\mathcal{T}_i, \\ \mathcal{T}_i = \sqrt{u_{i,x}^2 + u_{i,y}^2 + u_{i,z}^2}, \\ u_{i,\phi} = \mathcal{J}_{i,\phi}, \\ u_{i,\theta} = \mathcal{J}_{i,\theta}, \\ u_{i,\psi} = \mathcal{J}_{i,\psi}. \end{cases} \tag{2.6}$$

Due to the coupling between attitude dynamics and trajectory dynamics, only the desired heading angle (yaw) ψ_d can be directly designed. Based on this designed heading angle, the desired pitch angle θ_d and desired roll angle ϕ_d are calculated as follows:

$$\begin{cases} \phi_d = \arcsin\left(\dfrac{\upsilon_{i,x}\sin\psi_d - \upsilon_{i,y}\cos\psi_d}{\mathcal{T}_i}\right), \\ \theta_d = \arctan\left(\dfrac{u_{i,x}\cos\psi_d + u_{i,y}\sin\psi_d}{u_{i,z}}\right). \end{cases} \tag{2.7}$$

Let $\upsilon^*_{i,\tau}$ denote the saturation limit of the control input $\upsilon_{i,\tau}$ which corresponds to the i-th UAV. In order to effectively handle the issue of input saturation, the control signal $u_{i,\tau}$ is constrained as follows:

$$u_{i,\tau} = \begin{cases} \upsilon^*_{i,\tau} & \upsilon_{i,\tau} \geq \upsilon^*_{i,\tau}, \\ \upsilon_{i,\tau} & -\upsilon^*_{i,\tau} \leq \upsilon_{i,\tau} \leq \upsilon^*_{i,\tau}, \\ -\upsilon^*_{i,\tau} & \upsilon_{i,\tau} \leq -\upsilon^*_{i,\tau}. \end{cases} \tag{2.8}$$

This formulation ensures that the input signal $u_{i,\tau}$ remains within the predefined bounds, thereby mitigating the effects of input saturation on the control system.

The position tracking error is defined as follows:

$$z_{i,\tau} = \sum_{j=1}^{N} a_{ij}((p_{i,\tau} - o_{i,\tau}) - (p_{j,\tau} - o_{j,\tau})) + b_i(p_{i,\tau} - o_{i,\tau} - p_{d,\tau}), \tag{2.9}$$

where $o_{i,\tau}$ denotes the deviation of the i-th QUAV in the τ direction from the desired state trajectory $p_{d,\tau}$.

Control objective: Through the control design, the formation system dynamic can track the designed trajectory in a certain formation in a predefined-time with input-saturation and bounded disturbance. Moreover, according to the properties of the function tanh, singularities can be avoided, and nonsingular PTC of the QUAVF can be achieved.

Lemma 1 *(see [19]) For the nonlinear system (2.1), if there exists a radially unbounded positive definite continuously differentiable function V that satisfies:*

$$\dot{V} \leq -\frac{\pi}{\eta T_d}V^{1+\frac{\eta}{2}} - \frac{\iota\pi}{\eta T_d}V^{1-\frac{\eta}{2}} + \Delta, \tag{2.10}$$

where $T_d > 0$, η, ι are control parameters with $0 < \eta < 1$, $\iota = \sqrt{2} + 1$, and Δ is a non-negative constant related to system uncertainties, the nonlinear system is said to be practically prescribed-time stable [38]. Moreover, the system's stabilization time upper bound is $T_s = T_d$, and the trajectory convergence domain is given by the following:

$$\Omega_x = \left\{x : V < \frac{2\eta T_d\Delta}{\pi}\right\}. \tag{2.11}$$

Lemma 2. (Young's inequality) *For any variables $x_1, x_2 \in \mathbb{R}$, the following inequality holds:*

$$|x_1|^p|x_2|^q \leq \frac{p}{p+q}m|x_1|^{p+q} + \frac{q}{p+q}m^{-\frac{p}{q}}|x_2|^{p+q}, \tag{2.12}$$

where $p > 0$, $q > 0$, and $m > 0$ are constants.

Lemma 3. *For any variable $x \in \mathbb{R}$, the following inequality is true:*

$$|x| - x\tanh\left(\frac{x}{\varsigma}\right) \leq \kappa\varsigma, \tag{2.13}$$

where $\kappa = 0.2785$, and $\varsigma > 0$ is a control design parameter.

Lemma 4. *For any non-negative variables x_1, x_2, x_3, and $x_4 \leq x_3$:*

$$x_1^p(x_2 - x_1) \leq \frac{1}{1+p}(x_2^{1+p} - x_1^{1+p}), \quad (2.14)$$

$$(x_3 - x_4)^q \geq x_4^q - x_3^q, \quad (2.15)$$

where $p > 0$ and $q \geq 1$ are constants.

Lemma 5. (Sum inequalities) *For any variable $x_i \in \mathbb{R}$ (i = 1,2,...,n), the following inequalities hold:*

$$\sum_{i=1}^{n} |x_i|^p \geq \left(\sum_{i=1}^{n} |x_i|\right)^p \quad (2.16)$$

$$\sum_{i=1}^{n} |x_i|^q \geq n^{1-q}\left(\sum_{i=1}^{n} |x_i|\right)^q \quad (2.17)$$

where $0 < p \leq 1$ and $1 < q < \infty$ are constants.

3. Predefined-time control for input-saturated systems

In this section, the predefined-time controller is designed for QUAVF with input-saturation. And the predefined-time stability of the formation system is analysed.

3.1. Predefined-time control design

Based on the system dynamic (2.5), where the first equation describes the position dynamics and the second one describes the velocity dynamics affected by control input and disturbances, we construct an error system to achieve predefined-time formation under input saturation constraints. For position control, we introduce the tracking error $z_{i,\tau}$ from (2.9). For the velocity dynamics, we decompose $v_{i,\tau}$ by introducing two auxiliary signals: a filter output signal $\hat{\alpha}_{i,\tau}$ for predefined-time convergence and an anti-saturation signal $\chi_{i,\tau}$ to handle input constraints. This leads to the following:

$$\begin{cases} s_{i,\tau,1} = z_{i,\tau}, \\ s_{i,\tau,2} = v_{i,\tau} - \hat{\alpha}_{i,\tau} - \chi_{i,\tau}, \end{cases} \quad (3.1)$$

where $s_{i,\tau,1}$ and $s_{i,\tau,2}$ denote the system errors, with $z_{i,\tau}$ being the position tracking error defined in (2.9).

The filter is designed as follows:

$$\begin{aligned} \dot{\hat{\alpha}}_{i,\tau} = &- \frac{\bar{\gamma}\pi}{\bar{\lambda}\eta T_d}\xi_{i,\tau}^{1-\eta}\tanh\left(\frac{\bar{\gamma}\pi}{\bar{\lambda}\eta T_d}\frac{\xi_{i,\tau}^{2-\eta}}{\varsigma_{i,\tau}}\right) \\ &- \frac{\gamma\pi}{\lambda\eta T_d}\xi_{i,\tau}^{1+\eta} - \omega_{i,\tau}\xi_{i,\tau}, \end{aligned} \quad (3.2)$$

where $\xi_{i,\tau} = \hat{\alpha}_{i,\tau} - \alpha_{i,\tau}$ denotes the filter error, and $\alpha_{i,\tau}$ is the intermediate control signal that servers as the filter input. The constants are defined as follows: $\gamma = (24N)^{\frac{\eta}{2}}$, $\bar{\gamma} = 1 + \sqrt{2}, \lambda = 2^{1+\frac{\eta}{2}}, \bar{\lambda} = 2^{1-\frac{\eta}{2}}$. The filter's initial value is set to $\hat{\alpha}_{i,\tau}(0) = \alpha_{i,\tau}(0)$, and $\omega_{i,\tau}$ is a design parameter that satisfies $\omega_{i,\tau} \geq 1$.

The dynamics of the auxiliary signal is designed as follows:

$$\dot{\chi}_{i,\tau} = - \frac{\gamma_\chi\pi}{\lambda\eta T_d}\chi_{i,\tau}^{1+\eta} - \frac{\bar{\gamma}\pi}{\bar{\lambda}\eta T_d}\chi_{i,\tau}^{1-\eta} - \varpi_{i,\tau}\chi_{i,\tau} + g_\tau(u_{i,\tau} - \upsilon_{i,\tau}), \quad (3.3)$$

where $\gamma_\chi = (6N)^{\frac{\eta}{2}}$, and $\varpi_{i,\tau} \geq g_\tau^2$ is an auxiliary signal design parameter. Additionally, the initial value is set to $\chi_{i,\tau}(0) = 0$. According to (2.6), $u_{i,\tau} - \upsilon_{i,\tau}$ is bounded, meaning there exists a constant $\upsilon_{i,\tau}^*$ such that $|u_{i,\tau} - \upsilon_{i,\tau}| \leq \upsilon_{i,\tau}^*$.

Considering (2.5)–(2.9) and (3.1)–(3.3), the error dynamic equations can be rewritten as follows:

$$\begin{cases} \dot{s}_{i,\tau,1} = L_i(s_{i,\tau,2} + \xi_{i,\tau} + \alpha_{i,\tau} + \chi_{i,\tau}) + F_{i,\tau,1}, \\ \dot{s}_{i,\tau,2} = g_\tau\upsilon_{i,\tau} + F_{i,\tau,2} + d_{i,\tau}, \end{cases} \quad (3.4)$$

where $L_i = \sum_{j=1}^{N} a_{ij} + b_i$, and $F_{i,\tau,2} = f_{i,\tau} - \dot{\hat{\alpha}}_{i,\tau} + \frac{\gamma_\chi\pi}{\lambda\eta T_d}\chi_{i,\tau}^{1+\eta} + \frac{\bar{\gamma}\pi}{\bar{\lambda}\eta T_d}\chi_{i,\tau}^{1-\eta} + \varpi_{i,\tau}\chi_{i,\tau}$. Additionally, $F_{i,\tau,1} = -L_i\dot{o}_{i,\tau} - \sum_{j=1}^{N} a_{ij}(v_{j,\tau} - \dot{o}_{j,\tau}) - b_i\dot{p}_{d,\tau}$. Due to unknown parameters such as air resistance coefficients, the nonlinear terms $F_{i,\tau,k}$ are unknown continuous functions. According to the RBF-NN theorem, it can be deduced that

$$F_{i,\tau,k} = \vartheta_{i,\tau,k}^T\varphi_{i,\tau,k} + \varepsilon_{i,\tau,k}, \quad (3.5)$$

where $\|\vartheta_{i,\tau,k}\| \leq \vartheta_{i,\tau,k}^*$, and $|\varepsilon_{i,\tau,k}| \leq \varepsilon_{i,\tau,k}^*$.

First step: Design the following Lyapunov function:

$$V_{i,\tau,1} = \frac{1}{2}s_{i,\tau,1}^2 + \frac{1}{2}\tilde{\Lambda}_{i,\tau}^2, \quad (3.6)$$

where $\tilde{\Lambda}_{i,\tau} = \Lambda_{i,\tau} - \hat{\Lambda}_{i,\tau}$, and

$$\Lambda_{i,\tau} = \max\{\vartheta_{i,\tau,1}^{*2}, \varepsilon_{i,\tau,1}^{*2}, \vartheta_{i,\tau,2}^{*2}, \varepsilon_{i,\tau,2}^{*2}, d_{i,\tau}^{*2}, 1\}.$$

By taking the derivative, the following equality can be obtained:

$$\begin{aligned} \dot{V}_{i,\tau,1} &= s_{i,\tau,1}\dot{s}_{i,\tau,1} - \tilde{\Lambda}_{i,\tau}\dot{\hat{\Lambda}}_{i,\tau} \\ &= s_{i,\tau}\left(L_i\left(s_{i,\tau 2} + \xi_{i,\tau} + \alpha_{i,\tau} + \chi_{i,\tau}\right)\right. \\ &\quad \left. + \vartheta_{i,\tau,1}^T\varphi_{i,\tau,1} + \varepsilon_{i,\tau,1}\right) - \tilde{\Lambda}_{i,\tau}\dot{\hat{\Lambda}}_{i,\tau}. \end{aligned} \quad (3.7)$$

Applying Young's inequality, the following inequalities can be obtained:

$$L_i s_{i,\tau,1}(s_{i,\tau,2}+\xi_{i,\tau}) \leq \Lambda_{i,\tau}L_i^2 s_{i,\tau,1}^2+\frac{1}{2}\Lambda_{i,\tau}s_{i,\tau,2}^2+\frac{1}{2}\xi_{i,\tau}^2, \quad (3.8)$$

$$s_{i,\tau,1}(\vartheta_{i,\tau,1}^T\varphi_{i,\tau,1}+\varepsilon_{i,\tau,1}) \leq \Lambda_{i,\tau}s_{i,\tau,1}^2\varphi_{i,\tau,1}^T\varphi_{i,\tau,1}+\Lambda_{i,\tau}s_{i,\tau,1}^2+\frac{1}{2}. \quad (3.9)$$

Substituting the above inequalities into (3.7) leads to the following:

$$\begin{aligned}\dot V_{i,\tau,1} \leq\ & s_{i,\tau,1}\left(L_i\left(s_{i,\tau,2}^2+\xi_{i,\tau}\right)+\rho_{i,\tau,1}\Lambda_{i,\tau}s_{i,\tau,1}\right)\\ &-\tilde\Lambda_{i,\tau}\left(\dot{\hat\Lambda}_{i,\tau}-\rho_{i,\tau,1}\Lambda_{i,\tau}s_{i,\tau,1}^2\right)+\tfrac{1}{2}\Lambda_{i,\tau}s_{i,\tau,2}^2+\tfrac{1}{2}\xi_{i,\tau}^2+\tfrac{1}{2},\end{aligned} \quad (3.10)$$

where $\rho_{i,\tau,1}=1+L_i^2+\varphi_{i,\tau,1}^T\varphi_{i,\tau,1}$.

Design the intermediate control signal as follows:

$$\begin{aligned}\alpha_{i,\tau}=\ & L_i^{-1}\left[-\tfrac{\gamma\pi}{\lambda\eta T_d}s_{i,\tau,1}^{1+\eta}-\tfrac{\bar\gamma\pi}{\bar\lambda\eta T_d}s_{i,\tau,1}^{1-\eta}\tanh\left(\tfrac{\bar\gamma\pi}{\bar\lambda\eta T_d}\tfrac{s_{i,\tau}^{2-\eta}}{\varsigma i,\tau}\right)\right.\\ &\left.-L_i\chi_{i,\tau}-\rho_{i,\tau,1}\hat\Lambda_{i,\tau}s_{i,\tau,1}\right].\end{aligned} \quad (3.11)$$

Substituting into (3.10) leads to the following:

$$\begin{aligned}\dot V_{i,\tau,1}\ &\leq -\tfrac{\gamma\pi}{\lambda\eta T_d}s_{i,\tau,1}^{2+\eta}-\tfrac{\bar\gamma\pi}{\bar\lambda\eta T_d}s_{i,\tau,2}^{2-\eta}\tanh\left(\tfrac{\bar\gamma\pi}{\bar\lambda\eta T_d}\tfrac{S_{i,\tau}^{2-\eta}}{\varsigma i,\tau}\right)\\ &-\hat\Lambda_{i,\tau}\left(\dot{\hat\Lambda}_{i,\tau}-\rho_{i,\tau,1}s_{i,\tau,1}^2\right)\\ &+\tfrac{1}{2}\Lambda_{i,\tau}s_{i,\tau,2}^2+\tfrac{1}{2}\xi_{i,\tau}^2+\Delta_{i,\tau,1},\end{aligned} \quad (3.12)$$

where $\Delta_{i,\tau,1}=\frac{1}{2}$.

Second step: design the following Lyapunov function:

$$V_{i,\tau,2}=V_{i,\tau,1}+\frac{1}{2}s_{i,\tau,2}^2+\frac{1}{2}\xi_{i,\tau}^2. \quad (3.13)$$

Taking the following derivative:

$$\begin{aligned}\dot V_{i,\tau,2}\ &=\dot V_{i,\tau,1}+s_{i,\tau,2}\dot s_{i,\tau,2}+\xi_{i,\tau}\dot\xi_{i,\tau}\\ &=\dot V_{i,\tau,1}+s_{i,\tau,2}\left(g_\tau\upsilon_{i,\tau}+\vartheta_{i,\tau,2}^T\varphi_{i,\tau,2}+\varepsilon_{i,\tau,2}+d_{i,\tau}\right)\\ &-\tfrac{\gamma\pi}{\lambda\eta T_d}\xi_{i,\tau}^{2+\eta}-\tfrac{\bar\gamma\pi}{\bar\lambda\eta T_d}\xi_{i,\tau}^{2-\eta}\tanh\left(\tfrac{\bar\gamma\pi}{\bar\lambda\eta T_d}\tfrac{S_{i,\tau}^{2-\eta}}{\varsigma i,\tau}\right)\\ &-\omega_{i,\tau}\xi_{i,\tau}^2-\xi_{i,\tau}\dot{\hat\alpha}_{i,\tau}.\end{aligned} \quad (3.14)$$

Applying Young's inequality (Lemma 2) leads to the following:

$$\begin{aligned}&s_{i,\tau,2}(\vartheta_{i,\tau,2}^T\varphi_{i,\tau,2}+\varepsilon_{i,\tau,2}+d_{i,\tau})\\ &\leq \Lambda_{i,\tau}s_{i,\tau,2}^2\varphi_{i,\tau,2}^T\varphi_{i,\tau,2}+2\Lambda_{i,\tau}s_{i,\tau,2}^2+\frac{3}{4},\end{aligned} \quad (3.15)$$

$$-\xi_{i,\tau}\dot\alpha_{i,\tau}\leq\frac{1}{2}\xi_{i,\tau}^2+\frac{1}{2}\alpha_{i,\tau}^{*2}. \quad (3.16)$$

Substituting the above inequalities into (3.14), and considering the definition of $\omega_{i,\tau}$,

$$\begin{aligned}\dot V_{i,\tau,2}\leq\ &-\frac{\gamma\pi}{\lambda\eta T_d}s_{i,\tau,1}^{2+\eta}-\frac{\bar\gamma\pi}{\bar\lambda\eta T_d}s_{i,\tau,1}^{2-\eta}\tanh\left(\frac{\bar\gamma\pi}{\bar\lambda\eta T_d}\frac{S_{i,\tau}^{2-\eta}}{\varsigma i,\tau}\right)\\ &-\tilde\Lambda_{i,\tau}\left(\dot{\hat\Lambda}_{i,\tau}-\sum_{k=1}^{2}\rho_{i,\tau,k}s_{i,\tau,k}^2\right)\\ &+s_{i,\tau,2}\left(g\upsilon_{i,\tau}+\rho_{i,\tau,2}\hat\Lambda_{i,\tau}s_{i,\tau,2}\right)+\Delta_{i,\tau,2}\\ &-\frac{\gamma\pi}{\lambda\eta T_d}s_{i,\tau}^{2+\eta}-\frac{\bar\gamma\pi}{\bar\lambda\eta T_d}s_{i,\tau}^{2-\eta}\tanh\left(\frac{\bar\gamma\pi}{\bar\lambda\eta T_d}\frac{\xi_{i,\tau}^{2-\eta}}{\varsigma i,\tau}\right),\end{aligned} \quad (3.17)$$

where $\rho_{i,\tau,2}=\frac{3}{2}+\varphi_{i,\tau,2}^T\rho_{i,\tau,2}$, $\Delta_{i,\tau,2}=\Delta_{i,\tau,1}+\frac{1}{2}\alpha_{i,\tau}^{*2}+\frac{3}{4}$.

Design the control signal and adaptive law as follows:

$$\begin{aligned}\upsilon_{i,\tau}=\ & g_\tau^{-1}\left[-\tfrac{\gamma\pi}{\lambda\eta T_d}s_{i,\tau,2}^{1+\eta}-\tfrac{\bar\gamma\pi}{\bar\lambda\eta T_d}s_{i,\tau,2}^{1-\eta}\tanh\left(\tfrac{\bar\gamma\pi}{\bar\lambda\eta T_d}\tfrac{s_{i,\tau,2}^{2-\eta}}{\varsigma i,\tau}\right)\right.\\ &\left.-\rho_{i,\tau,2}\hat\Lambda_{i,\tau}s_{i,\tau,2}\right],\end{aligned} \quad (3.18)$$

$$\dot{\hat\Lambda}_{i,\tau}=\ -\tfrac{h\gamma\pi}{\lambda\eta T_d}\hat\Lambda_{i,\tau}^{1+\eta}-\tfrac{\bar h(\bar\gamma\pi)}{\bar\lambda\eta T_d}\hat\Lambda_{i,\tau}^{1-\eta}+\sum_{k=1}^{2}\rho_{i,\tau,k}s_{i,\tau,k}^2, \quad (3.19)$$

where $h=2+\eta$, $\bar h=2-\eta$. The initial value of the adaptive parameter $\hat\Lambda_{i,\tau}$ is set to $\hat\Lambda_{i,\tau}(0)>0$.

3.2. Stability analysis

By substituting Eqs (3.18) and (3.19) into (3.17), the following inequality is obtained:

$$\begin{aligned}\dot V_{i,\tau,2}\leq\ & -\tfrac{\gamma\pi}{\lambda\eta T_d}\sum_{k=1}^{2}s_{i,\tau,k}^{2+\eta}\\ &-\tfrac{\bar\gamma\pi}{\bar\lambda\eta T_d}\sum_{k=1}^{2}s_{i,\tau,k}^{2-\eta}\tanh\left(\frac{\bar\gamma\pi}{\bar\lambda\eta T_d}\frac{s_{i,\tau,k}^{2-\eta}}{\varsigma i,\tau}\right)\\ &-\tfrac{\gamma\pi}{\lambda\eta T_d}\xi_{i,\tau}^{2-\eta}-\tfrac{\bar\gamma\pi}{\bar\lambda\eta T_d}\xi_{i,\tau}^{2-\eta}\tanh\left(\tfrac{\bar\gamma\pi}{\bar\lambda\eta T_d}\tfrac{\xi_{i,\tau}^{2-\eta}}{\varsigma i,\tau}\right)\\ &+h\tfrac{\gamma\pi}{\lambda\eta T_d}\widetilde\Lambda_{i,\tau}\hat\Lambda_{i,\tau}^{1+\eta}+\bar h\tfrac{\bar\gamma\pi}{\bar\lambda\eta T_d}\widetilde\Lambda_{i,\tau}\hat\Lambda_{i,\tau}^{1-\eta}\\ &+\Delta_{i,\tau,2}.\end{aligned} \quad (3.20)$$

By considering (3.17), it can be obtained that $\frac{h\gamma\pi}{\lambda\eta T_d}, \frac{h\bar\gamma\pi}{\bar\lambda\eta T_d}>0$, $\sum_{k=1}^{2}\rho_{i,\tau,k}s_{i,\tau,k}^2>0$. It's obvious that $\hat\Lambda$ is continuous. Let $\hat\Lambda(0)>0$, and suppose there exists $\hat\Lambda(t_2)<0$ where $t_2>0$. Then, it can deduce that there exist $t_1\in(0,t_2)$ such that

$$\begin{cases}\hat\Lambda(t_1)=0,\\ \hat\Lambda(t)<0, t\in(t_1,t_2].\end{cases} \quad (3.21)$$

Thus, according to the form of (3.17), it should be noted that for $t \in (t_1, t_2]$, $\dot{\hat{\Lambda}} > 0$ holds. Then, integrating $\dot{\hat{\Lambda}}$ with respect to time from t_1 to t_2 yields the following:

$$\int_{t_1}^{t_2} \dot{\hat{\Lambda}} dt = \hat{\Lambda}(t_2) - \hat{\Lambda}(t_1) = \hat{\Lambda}(t_2) > 0. \tag{3.22}$$

Then, it contradicts the hypothesis. Thus, for $\hat{\Lambda}(0) > 0$, $\hat{\Lambda}(t) > 0$ for $t > 0$.

For the terms $\widetilde{\Lambda}_{i,\tau}\hat{\Lambda}_{i,\tau}^{1+\eta}$ and $\widetilde{\Lambda}_{i,\tau}\hat{\Lambda}_{i,\tau}^{1-\eta}$, according to Lemma 4, the following inequalities can be obtained:

$$\begin{aligned} \widetilde{\Lambda}_{i,\tau}\hat{\Lambda}_{i,\tau}^{1+\eta} &\leq \tfrac{1}{h}\left(\Lambda_{i,\tau}^{2+\eta} - \hat{\Lambda}_{i,\tau}^{2+\eta}\right) \\ &\leq \tfrac{1}{h}\left(2\Lambda_{i,\tau}^{2+\eta} - \widetilde{\Lambda}_{i,\tau}^{2+\eta}\right), \end{aligned} \tag{3.23}$$

$$\begin{aligned} \widetilde{\Lambda}_{i,\tau}\hat{\Lambda}_{i,\tau}^{1-\eta} &\leq \tfrac{1}{h}\left(\Lambda_{i,\tau}^{2-\eta} - \hat{\Lambda}_{i,\tau}^{2-\eta}\right) \\ &\leq \tfrac{1}{h}\left(2\Lambda_{i,\tau}^{2-\eta} - \widetilde{\Lambda}_{i,\tau}^{2-\eta}\right). \end{aligned} \tag{3.24}$$

It should be noticed that $-\frac{\bar{\gamma}\pi}{\bar{\lambda}\eta T_d} s_{i,\tau,k}^{2-\eta}\tanh\left(\frac{\bar{\gamma}\pi}{\bar{\lambda}\eta T_d}\frac{s_{i,\tau,k}^{2-\eta}}{\varsigma i,\tau}\right)$ and $-\frac{\bar{\gamma}\pi}{\bar{\lambda}\eta T_d}\xi_{i,\tau}^{2-\eta}\tanh\left(\frac{\bar{\gamma}\pi}{\bar{\lambda}\eta T_d}\frac{\xi_{i,\tau}^{2-\eta}}{\varsigma i,\tau}\right)$ need to be further processed. According to Lemma 3, the following inequalities can be deduced:

$$-\tfrac{\bar{\gamma}\pi}{\bar{\lambda}\eta T_d} s_{i,\tau,k}^{2-\eta}\tanh\left(\tfrac{\bar{\gamma}\pi}{\bar{\lambda}\eta T_d}\tfrac{s_{i,\tau,k}^{2-\eta}}{\varsigma i,\tau}\right) \leq -\tfrac{\bar{\gamma}\pi}{\bar{\lambda}\eta T_d} s_{i,\tau,k}^{2-\eta} + \kappa\varsigma_{i,\tau}, \tag{3.25}$$

$$-\tfrac{\bar{\gamma}\pi}{\bar{\lambda}\eta T_d}\xi_{i,\tau}^{2-\eta}\tanh\left(\tfrac{\bar{\gamma}\pi}{\bar{\lambda}\eta T_d}\tfrac{\xi_{i,\tau}^{2-\eta}}{\varsigma i,\tau}\right) \leq -\tfrac{\bar{\gamma}\pi}{\bar{\lambda}\eta T_d}\xi_{i,\tau}^{2-\eta} + \kappa\varsigma_{i,\tau}. \tag{3.26}$$

By substituting inequalities (3.23)–(3.26) into (3.20), the following inequality can be obtained:

$$\begin{aligned} \dot{V}_{i,\tau,2} \leq\; & -\tfrac{\gamma\pi}{\lambda\eta T_d}\sum_{k=1}^{2} s_{i,\tau,k}^{2+\eta} - \frac{\gamma\pi}{\lambda\eta T_d}\widetilde{\Lambda}_{i,\tau}^{2+\eta} - \frac{\gamma\pi}{\lambda\eta T_d}\xi_{i,\tau}^{2+\eta} \\ & -\tfrac{\bar{\gamma}\pi}{\bar{\lambda}\eta T_d}\sum_{k=1}^{2} s_{i,\tau,k}^{2-\eta} - \frac{\bar{\gamma}\pi}{\bar{\lambda}\eta T_d}\widetilde{\Lambda}_{i,\tau}^{2-\eta} - \frac{\bar{\gamma}\pi}{\bar{\lambda}\eta T_d}\xi_{i,\tau}^{2-\eta} + \Delta_{i,\tau}, \end{aligned} \tag{3.27}$$

where $\Delta_{i,\tau} = \Delta_{i,\tau,2} + 3\kappa\varsigma_{i,\tau} + \frac{2\gamma\pi}{\lambda\eta T_d}\Lambda_{i,\tau}^{2+\eta} + \frac{2\bar{\gamma}\pi}{\bar{\lambda}\eta T_d}\Lambda_{i,\tau}^{2-\eta}$.

For the QUAVF, the Lyapunov function is constructed as follows:

$$\begin{aligned} V &= \sum_{i=1}^{N}\sum_{\tau\in\Xi} V_{i,\tau,2} \\ &= \sum_{i=1}^{N}\sum_{\tau\in\Xi}\left(\sum_{k=1}^{2}\frac{1}{2}s_{i,\tau,k}^2 + \frac{1}{2}\widetilde{\Lambda}_{i,\tau}^2 + \frac{1}{2}\xi_{i,\tau}^2\right). \end{aligned} \tag{3.28}$$

Differentiating the above Eq (3.30) yields the following:

$$\begin{aligned} \dot{V} \leq \sum_{i=1}^{N}\sum_{\tau\in\Xi}\Bigg[& -\frac{\gamma\pi}{\lambda\eta T_d}\sum_{k=1}^{2} s_{i,\tau,k}^{2+\eta} - \frac{\gamma\pi}{\lambda\eta T_d}\tilde{\Lambda}_{i,\tau}^{2+\eta} - \frac{\gamma\pi}{\lambda\eta T_d}\xi_{i,\tau}^{2+\eta} \\ & -\frac{\bar{\gamma}\pi}{\bar{\lambda}\eta T_d}\sum_{k=1}^{2} S_{i,\tau,k}^{2-\eta} - \frac{\bar{\gamma}\pi}{\bar{\lambda}\eta T_d}\tilde{\Lambda}_{i,\tau}^{2-\eta} - \frac{\bar{\gamma}\pi}{\bar{\lambda}\eta T_d}\xi_{i,\tau}^{2-\eta} + \Delta_{i,\tau}\Bigg]. \end{aligned} \tag{3.29}$$

Taking the derivative of the Lyapunov function, and applying Lemma 5, the following can be obtained:

$$-\tfrac{\gamma\pi}{\lambda\eta T_d}\sum_{i=1}^{N}\sum_{\tau\in\Xi}\left(\sum_{k=1}^{2} s_{i,\tau,k}^{2+\eta} + \widetilde{\Lambda}_{i,\tau}^{2+\eta} + \xi_{i,\tau}^{2+\eta}\right) \leq -\frac{\pi}{\eta T_d}V^{1+\frac{\eta}{2}}, \tag{3.30}$$

$$-\tfrac{\bar{\gamma}\pi}{\bar{\lambda}\eta T_d}\sum_{i=1}^{N}\sum_{\tau\in\Xi}\left(\sum_{k=1}^{2} s_{i,\tau,k}^{2-\eta} + \widetilde{\Lambda}_{i,\tau}^{2+\eta} + \xi_{i,\tau}^{2-\eta}\right) \leq -\frac{\bar{\gamma}\pi}{\eta T_d}V^{1-\frac{\eta}{2}}. \tag{3.31}$$

Thus, (3.29) can be rewritten as follows:

$$\dot{V} \leq -\tfrac{\pi}{\eta T_d}V^{1+\frac{\eta}{2}} - \tfrac{\bar{\gamma}\pi}{\eta T_d}V^{1-\frac{\eta}{2}} + \Delta, \tag{3.32}$$

where $\Delta = \sum_{i=1}^{N}\sum_{\tau\in\Xi}\Delta_{i,\tau}$.

Based on the definition of V, the variables $s_{i,\tau,1}$, $\tilde{\Lambda}_{i,\tau}$, $s_{i,\tau,2}$, and $\xi_{i,\tau}$ are bounded and achieve predefined-time stability. From (3.1), the error system $z_{i,\tau}$ and $v_{i,\tau} - \hat{\alpha}_{i,\tau} - \chi_{i,\tau}$ are also bounded and converge to zero. Since $\Lambda_{i,\tau}^*$ is constant and $\alpha_{i,\tau}$ is bounded, both $\hat{\Lambda}_{i,\tau}$ and $\hat{\alpha}_{i,\tau}$ remain bounded. For the auxiliary system $\chi_{i,\tau}$, its stability is analyzed through $s_{i,\tau,2} = \upsilon_{i,\tau} - \hat{\alpha}_{i,\tau} - \chi_{i,\tau}$.

Consider the dynamics of the auxiliary system and construct the following Lyapunov function:

$$V_\chi = \sum_{i=1}^{N}\sum_{\tau\in\Xi}\frac{1}{2}\chi_{i,\tau}^2. \tag{3.33}$$

Differentiating this function yields the following:

$$\begin{aligned} \dot{V}_\chi =\; & \sum_{i=1}^{N}\sum_{\tau\in\mathcal{E}}\chi_{i,\tau}\dot{\chi}_{i,\tau} \\ =\; & \sum_{i=1}^{N}\sum_{\tau\in\mathcal{E}}\left(-\frac{\gamma\pi}{\lambda\eta T_d}\chi_{i,\tau}^{2+\eta} - \frac{\bar{\gamma}\pi}{\bar{\lambda}\eta T_d}\chi_{i,\tau}^{2-\eta}\right) \\ & + \sum_{i=1}^{N}\sum_{\tau\in\mathcal{E}}\left(-\varpi\chi_{i,\tau}^2 + g_\tau(u_{i,\tau} - \upsilon_{i,\tau})\chi_{i,\tau}\right). \end{aligned} \tag{3.34}$$

According to the Young's inequality (Lemma 2), the following inequalities can be obtained:

$$g_\tau(u_{i,\tau} - \upsilon_{i,\tau})\chi_{i,\tau} \leq g_\tau^2\chi_{i,\tau}^2 + \tfrac{1}{4}v_{i,\tau}^{*2}. \tag{3.35}$$

Substituting (3.35) into (3.34) yields the following:

$$\dot{V}_\chi \le \sum_{i=1}^{N}\sum_{\tau\in\mathcal{E}}\left(-\frac{\gamma_\chi \pi}{\lambda\eta T_d}\chi_{i,\tau}^{2+\eta} - \frac{\bar{\gamma}\pi}{\bar{\lambda}\eta T_d}\chi_{i,\tau}^{2-\eta} + \frac{1}{4}v_{i,\tau}^{*2}\right). \quad (3.36)$$

By substituting the above inequalities, it can be rewritten as follows:

$$\dot{V}_\chi \le -\frac{\pi}{\eta T_d}V_\chi^{1+\frac{\eta}{2}} - \frac{\bar{\gamma}\pi}{\eta T_d}T_d V_\chi^{1-\frac{\eta}{2}} + \Delta_\chi, \quad (3.37)$$

where $\Delta_\chi = \sum_{i=1}^{N}\sum_{\tau\in\Xi}\left(\frac{1}{4}v_{i,\tau}^{*2}\right)$.

Due to the stability analysis of (3.37), the auxiliary system achieves predefined-time stability. By (3.1), this ensures the boundedness of $v_{i,\tau}$. According to the controller (3.18) and input saturation (2.8), both $\upsilon_{i,\tau}$ and $u_{i,\tau}$ remain bounded. Therefore, the QUAVF system converges to a residual set within the predefined time T_d.

Remark: The QUAVF control method proposed in this paper achieves predefined-time stability and effective handling of the input saturation constraints. Unlike the finite-time or fixed-time control methods that rely on complex parameter tuning, our approach can allow users to directly set the upper bound of the stabilization time and facilitate easier practical deployment. Furthermore, in contrast to other the auxiliary systems that only ensure the asymptotic stability of auxiliary signals, the auxiliary system we designed can achieve predefined-time stability. Then, it is integrated into the distributed formation controller to effectively contribute to the predefined-time stabilization of the entire QUAVF.

4. Simulation

A 6-D QUAVF control problem is considered in the simulation. The parameters in the system dynamic of each UAV is shown as follows: mass $m = 1kg$, aerodynamic damping coefficients $\mathcal{K}_{i,\tau} = 0.01$, moments of inertia $\mathcal{I}_x = \mathcal{I}_y = 50\times10^{-3}kg{\cdot}m^2$, and $\mathcal{I}_z = 20\times10^{-3}kg{\cdot}m^2$. Additionally, the external disturbance is set as $\mathcal{D}_i = 0.01\sin(t)$.

The desired formation pattern is a square with side length 4 m in the xy-plane. UAV1 (leader) is positioned at (-2, 2), while UAV2-4 are at (2, 2), (-2, -2), and (2, -2) respectively. The initial positions slightly deviate from the desired pattern: UAV1 at (-2.1, 3.1), UAV2 at (2.1, 3.1), UAV3 at (-2.1, -1.1), and UAV4 at (2.1, -1.1), with zero initial altitude and attitude angles for all UAVs.

The control parameters are defined by the ratio parameter $\eta = \frac{6}{101}$ and the predefined time $T_d = 10\ s$. The other controller parameters are set as: the scaling factors $\varsigma_{i,\tau} = 0.005$ in the virtual control design (3.11) and $\varsigma_{i,\tau} = 0.001$ in the control input design (3.18), $\omega_{i,\tau} = 12$ for x and y directions, $\omega_{i,\tau} = 15$ for z direction, $\omega_{i,\tau} = 5$ for attitude angles, and $\bar{\omega}_{i,\tau} = 1$ for all velocity controllers.

The communication topology between the leader and followers is illustrated in Figure 1. Figure 2 shows the 3D trajectories of the QUAVF. The formation stabilizes before the predefined time $T_d = 10s$.

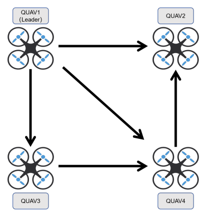

Figure 1. Communication topology.

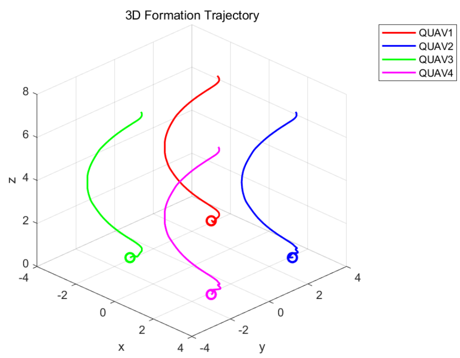

Figure 2. 3D trajectories.

Figure 3 presents the position tracking in all coordinates, where the leader follows ($x_d = \sin(0.5t), y_d = \cos(0.5t)$) in the xy-plane and the $z_d = 0.5t$ in z-direction. As shown in Figure 4, the tracking errors converge within $T_d = 10\ s$. Figure 5 shows that under the proposed auxiliary system, the control signals strictly respect their saturation constraints $\upsilon_{i,x}^* = \upsilon_{i,y}^* = 4$ and $\upsilon_{i,z}^* = 11$ while maintaining the formation performance.

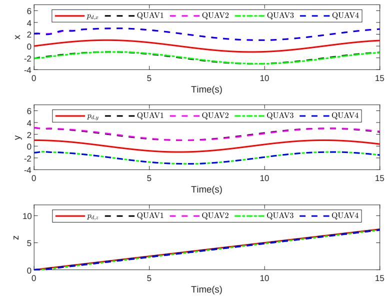

Figure 3. Position tracking.

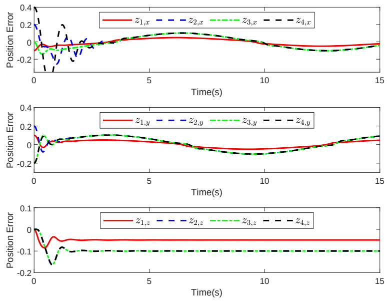

Figure 4. Position errors.

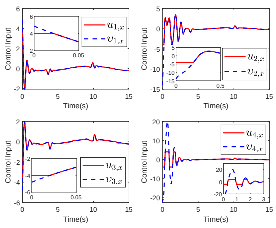

(a) x-direction

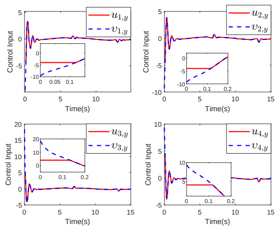

(b) y-direction

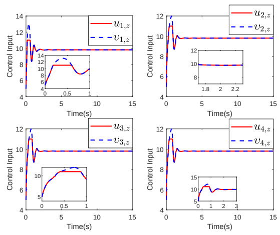

(c) z-direction

Figure 5. Translation control inputs.

Figure 6 displays the attitude tracking errors for roll, pitch, and yaw angles. Figures 7–9 show the attitude control results where the yaw angle converges to $\psi_d = 0$, while the roll and pitch angles track their computed desired values derived from translational control (2.7). All attitude control inputs respect the bounds $\upsilon^*_{i,\phi} = \upsilon^*_{i,\theta} = \upsilon^*_{i,\psi} = 1$.

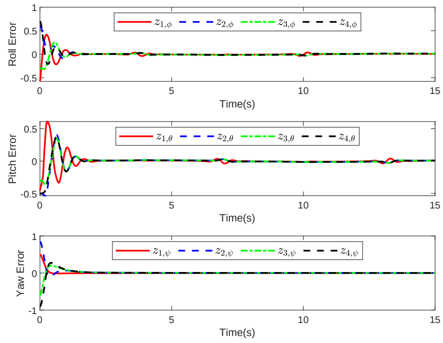

Figure 6. Attitude errors.

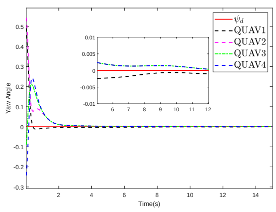

(a) Tracking

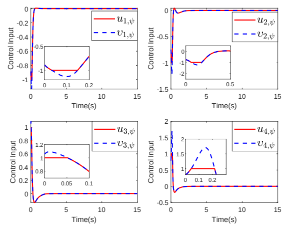

(b) Control

Figure 7. Yaw angle control.

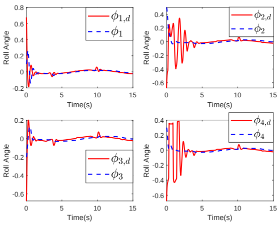

(a) Tracking

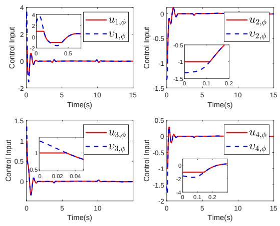

(b) Control

Figure 8. Roll angle control.

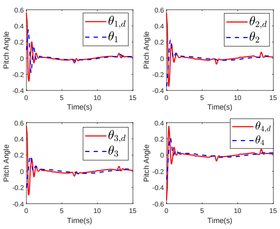

(a) Tracking

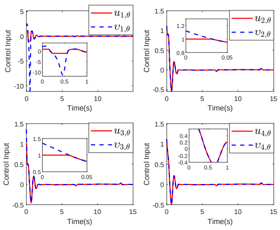

(b) Control

Figure 9. Pitch angle control.

The simulation results comprehensively validate the effectiveness of the proposed control strategy under the input saturation constraints ($\upsilon^*_{i,x} = \upsilon^*_{i,y} = 4$, $\upsilon^*_{i,z} = 11$, and $\upsilon^*_{i,\phi} = \upsilon^*_{i,\theta} = \upsilon^*_{i,\psi} = 1$). Both the position and attitude tracking errors converge to a neighborhood of zero within the predefined time $T_d = 10\ s$ (Figures 4 and 6), thereby demonstrating accurate formation control. The predefined-time auxiliary system effectively handles the input saturation while maintaining the formation stability. Moreover, by setting these saturation bounds below the actual physical limits, the method provides a practical solution that prevents system overload and ensures a safe operation in real applications.

5. Conclusions

This paper proposed a PTC approach for QUAVF systems under input saturation. Unlike conventional finite-time or fixed-time control strategies, which often depend on complex parameter tuning and lack flexibility in the stabilization time, our method enables the user to directly specify the upper bound of convergence time. Moreover, by incorporating a predefined-time auxiliary system, we mitigate the negative effects of input saturation, thus ensuring both stability and rapid convergence within a defined timeframe. This study addresses a critical gap in existing research.

The simulation demonstrated the effectiveness of the proposed method, thereby showing its ability to maintain stability of QUAVF even under input constraints. This work advances the theoretical understanding of predefined-time control while providing a robust solution for the deployment of QUAVF systems in complex environments.

Future research directions are threefold: first, refining the auxiliary system design to accommodate a broader range of operational conditions and exploring the application of this framework to other multi-agent systems; second, investigating the impact of communication topology and networking effects, which are particularly relevant for underactuated quadrotor systems; third, conducting experimental validation on physical QUAV platforms to further demonstrate the practical applicability of the proposed method. These extensions will enhance the versatility and real-world applicability of our approach.

Use of Generative-AI tools declaration

The authors declare they have used Artificial Intelligence (AI) tools in the creation of this article. AI tools were used for language editing purposes, including improving grammar, wording, sentence fluency, and readability of the manuscript.

Acknowledgments

This work was supported by the Natural Science Foundation of Shandong Province of China (ZR2023MF012), the National Natural Science Foundation of China (41927805, 41906177), the Hainan Provincial Joint Project of Sanya Yazhou Bay Science and Technology City (2021JJLH0061)and Sanya Science and Technology Special Fund (2022KJCX92). We sincerely appreciate these support.

Conflict of interest

The authors declare there is no conflict of interests.

References

1. H. Guo, M. Chen, S. Shi, Z. Han, M. Lungu, Distributed coordinated control for QUAVs with switching formation strategy, *IEEE Trans. Intell. Veh.*, **10** (2025), 3841–3851. https://doi.org/10.1109/TIV.2024.3466152
2. J. Scherer, S. Yahyanejad, S. Hayat, E. Yanmaz, T. Andre, A. Khan, et al., An autonomous multi-UAV system for search and rescue, *Proceedings of the first workshop on micro aerial vehicle networks, systems, and applications for civilian use*, 2015, 33–38. https://doi.org/10.1145/2750675.2750683
3. P. Garcia-Aunon, J. J. Roldán, A. Barrientos, Monitoring traffic in future cities with aerial swarms: developing and optimizing a behavior-based surveillance algorithm, *Cogn. Syst. Res.*, **54** (2019), 273–286. https://doi.org/10.1016/j.cogsys.2018.10.031

4. A. Hegde, D. Ghose, Multi-quadrotor distributed load transportation for autonomous agriculture spraying operations, *J. Guid. Control Dyn.*, **45** (2022), 944–951. https://doi.org/10.2514/1.G006608

5. Y. Hou, Y. Liu, S. Tong, Decentralized event-triggered fault-tolerant control for switched interconnected nonlinear systems with input saturation and time-varying full-state constraints, *IEEE Trans. Fuzzy Syst.*, **32** (2024), 3850–3860. https://doi.org/10.1109/TFUZZ.2024.3392632

6. S. P. Bhat, D. S. Bernstein, Finite-time stability of continuous autonomous systems, *SIAM J. Control Optim.*, **38** (2000), 751–766. https://doi.org/10.1137/S0363012997321358

7. H. Du, W. Zhu, G. Wen, D. Wu, Finite-time formation control for a group of quadrotor aircraft, *Aerosp. Sci. Technol.*, **69** (2017), 609–616. https://doi.org/10.1016/j.ast.2017.07.012

8. Y. Huang, W. Liu, B. Li, Y. Yang, B. Xiao, Finite-time formation tracking control with collision avoidance for quadrotor UAVs, *J. Franklin Inst.*, **357** (2020), 4034–4058. https://doi.org/10.1016/j.jfranklin.2020.01.014

9. Y. Niu, H. Ban, H. Zhang, W. Gong, F. Yu, Nonsingular terminal sliding mode based finite-time dynamic surface control for a quadrotor UAV, *Algorithms*, **14** (2021), 315. https://doi.org/10.3390/a14110315

10. P. Yang, A. Zhang, W. Bi, M. Li, Cooperative group formation control for multiple quadrotors system with finite- and fixed-time convergence, *ISA Trans.*, **138** (2023), 186–196. https://doi.org/10.1016/j.isatra.2023.03.029

11. J. Zhao, B. Zhang, Y. Hu, D. Yu, Z. Y. Sun, C. L. P. Chen, Prescribed performance-based switching tracking algorithm for dcdc buck power converter with nonaffine input and stochastic disturbance, *IEEE T. Syst. Man Cybern.-Syst.*, **55** (2025), 2759–2770. https://doi.org/10.1109/TSMC.2024.3515040

12. Z. Zuo, B. Tian, M. Defoort, Z. Ding, Fixed-time consensus tracking for multiagent systems with high-order integrator dynamics, *IEEE Trans. Autom. Control*, **63** (2018), 563–570. https://doi.org/10.1109/TAC.2017.2729502

13. Y. Liu, H. Li, R. Lu, Z. Zuo, X. Li, An overview of finite/fixed-time control and its application in engineering systems, *IEEE-CAA J. Auto. Sin.*, **9** (2022), 2106–2120. https://doi.org/10.1109/JAS.2022.105413

14. M. Huang, Q. Lu, A fixed-time hierarchical formation control strategy for multiquadrotors, *J. Rob.*, **2021** (2021), 9979713. https://doi.org/10.1155/2021/9979713

15. G. Cui, H. Xu, X. Chen, J. Yu, Fixed-time distributed adaptive formation control for multiple QUAVs with full-state constraints, *IEEE Trans. Aerosp. Electron. Syst.*, **59** (2023), 4192–4206. https://doi.org/10.1109/TAES.2023.3237784

16. Q. Miao, K. Zhang, B. Jiang, Fixed-time collision-free fault-tolerant formation control of multi-UAVs under actuator faults, *IEEE Trans. Cybern.*, **54** (2024), 3679–3691. https://doi.org/10.1109/TCYB.2024.3352251

17. D. Yu, S. Ma, Z. Wang, Y. Liu, C. L. P. Chen, Fixed-time attitude control for QUAV with stochastic disturbances: theory and experiment, *IEEE Trans. Ind. Electron.*, **71** (2024), 16484–16492. https://doi.org/10.1109/TIE.2024.3390730

18. Q. Li, Y. Chen, K. Liang, Predefined-time formation control of the quadrotor-UAV cluster'position system, *Appl. Math. Model.*, **116** (2023), 45–64. https://doi.org/10.1016/j.apm.2022.11.011

19. H. Xu, D. Yu, S. Sui, B. Xu, C. L. P. Chen, A practical predefined-time stability criterion and its application to uncertain nonlinear systems, *J. Syst. Sci. Complex.*, **37** (2024), 2556–2578. https://doi.org/10.1007/s11424-024-4051-x

20. J. Ni, L. Liu, Y. Tang, C. Liu, Predefined-time consensus tracking of second-order multiagent systems, *IEEE T. Syst. Man Cybern.-Syst.*, **51** (2019), 2550–2560. https://doi.org/10.1109/TSMC.2019.2916257

21. H. Liu, H. Tu, S. Huang, X. Zheng, Adaptive predefined-time sliding mode control for QUADROTOR formation with obstacle and inter-quadrotor avoidance, *Sensors*, **23** (2023), 2392. https://doi.org/10.3390/s23052392

22. X. Shao, G. Sun, W. Yao, J. Liu, L. Wu, Adaptive sliding mode control for quadrotor UAVs with input saturation, *IEEE/ASME Trans. Mech.*, **27** (2022), 1498–1509. https://doi.org/10.1109/TMECH.2021.3094575

23. X. Yan, M. Chen, Q. Wu, S. Shao, Adaptive neural tracking control for near-space vehicles with stochastic disturbances, *Int. J. Adv. Rob. Syst.*, **14** (2017), 1–10. https://doi.org/10.1177/1729881417703777
24. Y. F. Gao, X. M. Sun, C. Wen, W. Wang, Adaptive tracking control for a class of stochastic uncertain nonlinear systems with input saturation, *IEEE Trans. Autom. Control*, **62** (2017), 2498–2504. https://doi.org/10.1109/TAC.2016.2600340
25. R. Wang, J. Liu, Trajectory tracking control of a 6-DOF quadrotor UAV with input saturation via backstepping, *J. Franklin Inst.*, **355** (2018), 3288–3309. https://doi.org/10.1016/j.jfranklin.2018.01.039
26. Q. Xu, Z. Wang, Z. Zhen, Adaptive neural network finite time control for quadrotor UAV with unknown input saturation, *Nonlinear Dyn.*, **98** (2019), 1973–1998. https://doi.org/10.1007/s11071-019-05301-1
27. L. Wang, H. He, Z. Zeng, M. F. Ge, Model-independent formation tracking of multiple Euler–Lagrange systems via bounded inputs, *IEEE Trans. Cybern.*, **51** (2021), 2813–2823. https://doi.org/10.1109/TCYB.2019.2938398
28. D. Yu, J. Long, C. P. Chen, Z. Wang, Adaptive swarm control within saturated input based on nonlinear coupling degree, *IEEE T. Syst. Man Cybern.-Syst.*, **52** (2022), 4900–4911. https://doi.org/10.1109/TSMC.2021.3102587
29. R. Wang, J. Liu, Adaptive formation control of quadrotor unmanned aerial vehicles with bounded control thrust, *Chinese J. Aeronaut.*, **30** (2017), 807–817. https://doi.org/10.1016/j.cja.2017.01.007
30. A. Zhang, D. Zhou, M. Yang, P. Yang, Finite-time formation control for unmanned aerial vehicle swarm system with time-delay and input saturation, *IEEE Access*, **7** (2019), 5853–5864. https://doi.org/10.1109/ACCESS.2018.2889858
31. H. Xu, G. Cui, Q. Ma, Z. Li, Event-triggered distributed adaptive fixed-time formation control of QUAVs with input constraints, *IEEE Trans. Veh. Technol.*, **73** (2024), 6357–6367. https://doi.org/10.1109/TVT.2023.3345925
32. P. Jin, Q. Ma, J. Gu, Fixed-time practical antisaturation attitude tracking control of QUAV with prescribed performance: theory and experiments, *IEEE Trans. Aerosp. Electron. Syst.*, **60** (2024), 6050–6060. https://doi.org/10.1109/TAES.2024.3400177
33. Z. T. Dydek, A. M. Annaswamy, E. Lavretsky, Adaptive control of quadrotor UAVs: a design trade study with flight evaluations, *IEEE Trans. Control Syst. Technol.*, **21** (2013), 1400–1406. https://doi.org/10.1109/TCST.2012.2200104
34. J. Li, J. Liu, S. Huangfu, G. Cao, D. Yu, Leader-follower formation of light-weight UAVs with novel active disturbance rejection control, *Appl. Math. Modell.*, **117** (2023), 577–591. https://doi.org/10.1016/j.apm.2022.12.032
35. J. Li, D. Yu, W. Ma, J. J. R. Liu, Y. J. Liu, Cooperative control of air–ground swarms under DoS attacks via cloud–fog computing, *IEEE Trans. Network Sci. Eng.*, **11** (2024), 4278–4292. https://doi.org/10.1109/TNSE.2024.3409900
36. H. Xu, D. Yu, Z. Wang, K. H. Cheong, C. L. P. Chen, Nonsingular predefined time adaptive dynamic surface control for quantized nonlinear systems, *IEEE T. Syst. Man Cybern.-Syst.*, **54** (2024), 5567–5579. https://doi.org/10.1109/TSMC.2024.3407150
37. B. Niu, Y. Liu, G. Zong, Z. Han, J. Fu, Command filter-based adaptive neural tracking controller design for uncertain switched nonlinear output-constrained systems, *IEEE Trans. Cybern.*, **47** (2017), 3160–3171. https://doi.org/10.1109/TCYB.2016.2647626
38. H. Xu, D. Dong, D. Yu, Y. J. Liu, Predefined-time fuzzy adaptive control for spacecraft pose tracking with asymptotic error, *IEEE Trans. Fuzzy Syst.*, **33** (2025), 971–981. https://doi.org/10.1109/TFUZZ.2024.3502360